

Original Article

Knockdown of VDAC1 alleviates the cognitive dysfunction secondary to sepsis-associated encephalopathy

Mengmeng Cai^{1*}, Boxiang Du^{2*}, Yanna Si¹, Juanjuan Miao², Jianyun Ge², Jiejie Zhang², Jie Song², Hongguang Bao¹

¹Department of Anesthesiology, Affiliated Nanjing Hospital of Nanjing Medical University (Nanjing First Hospital), Nanjing, Jiangsu Province, China; ²Department of Anesthesiology, The Second Affiliated Hospital of Nantong University, Nantong, Jiangsu Province, China. *Equal contributors and co-first authors.

Received December 28, 2020; Accepted May 13, 2021; Epub July 15, 2021; Published July 30, 2021

Abstract: Sepsis-associated encephalopathy (SAE) is a serious and diffuse cerebral dysregulation with a high morbidity and mortality caused by sepsis. Mitophagy plays an important role in SAE, and microglial phagocytosis of apoptotic cells (efferocytosis) is the core of the brain regenerative response. Voltage dependent anion channel (VDAC1) is an important regulator of mitophagy. However, it remains unknown whether VDAC1 influences SAE progression by regulating mitophagy and efferocytosis. Herein, we explored the mechanism where knockdown of VDAC1 alleviated the cognitive dysfunction caused by sepsis-associated encephalopathy and further elucidated the underlying molecular mechanisms. SAE model in mice was established through caecal ligation and puncture (CLP). The increased mitophagy and decreased efferocytosis were observed by the transmission electron microscope (TEM) in the SAE model. Besides, immunoblot tests showed an interaction between autophagy and efferocytosis. Further behavior tests and TEM results indicated that knockdown of VDAC1 alleviated the cognitive dysfunction by decreasing the autophagy and increasing the efferocytosis in a PINK1/Parkin-dependent manner. Based on these results, we conclude that knockdown of VDAC1 alleviates the cognitive dysfunction in the CLP-induced SAE mouse model.

Keywords: VDAC1, PINK1/Parkin, mitophagy, efferocytosis, sepsis-associated encephalopathy

Introduction

Sepsis-associated encephalopathy (SAE) is defined as a serious and diffuse cerebral dysregulation caused by failure of defense system against microbial infection in systematically ill patients [1, 2]. Several clinical studies indicated that more than 50 percent of patients with sepsis had symptoms of SAE [3, 4]. It is reported that septic patients with neurological manifestations had a higher mortality rate ranging from 26% to 49% [5]. Several pathophysiological mechanisms for signal mediation have been reported, including alterations of the neuropsychiatric continuum related to the septic shock caused by the blood-brain barrier (BBB) dysfunction, activation of proinflammatory mediators, mitochondrial disruption by the excessive reactive oxygen species (ROS), imbalance of immune homeostasis, as

well as mitochondrial dysfunction [6-8]. However, more effort should be conducted to explore the mechanism of the pathogenesis of SAE for an early effective clinical intervention.

Mitophagy involves the clearance of impaired mitochondria, minimizing the subsequent cellular stress and preservation of the health mitochondria [9, 10]. Parkin, as a cytosolic ubiquitin ligase, and phosphatase and tension homolog deleted on chromosome 10-induced kinase 1 (PINK1) [10, 11] play an important role in mitophagy. Under the physiological condition, PINK1 exists in the outer membrane of mitochondria (OMM), which is quickly degraded by proteolytic enzymes [12]. During mitophagy, the activity of proteolytic enzymes responsible for the degradation of PINK1 is inhibited, leading to gathering of PINK1 in the damaged OMM [13]. PINK1 recruits Parkin from the cytoplasm

Decreasing the VDAC1 alleviated the cognitive dysfunction

to the damaged mitochondrial membrane [14]. VDAC1 works as a critical component of mitochondrial permeability transition pore (mPTP) [15]. When Parkin induces polyubiquitination on VDAC1 [16], the adaptor protein p62 accumulates on the depolarized mitochondrial matrix and then binds to LC3 [17]. The protein p62 mediates the ubiquitination substrate to enter the autophagosome and recruit the damaged mitochondria in lysosome to complete mitochondrial autophagy [18].

The efferocytosis is defined as process of the recognition and elimination of aging and apoptotic cells by phagocytes [19]. The macrophages, microglia and dendritic cells are the most common cells involved in efferocytosis [20, 21]. Efferocytosis is a cell removal mechanism differing from other forms of phagocytosis, which has several different phases: First, apoptotic cells are sensed by “Find-me” signal [22, 23]. Second, apoptotic cells are identified by “Eat-me” signal during the identification stage [24, 25]. In addition, they interact through “Don’t eat-me” signal, which is sent by living cells for resistance to phagocytosis [26, 27]. Phagocytosis stage includes the signaling pathways that regulate cytoskeletal rearrangement in phagocytes, such as toll-like receptor 4 (TLR4) and lipopolysaccharide receptor [28, 29]. Final digestion and degradation stages include the secretion of anti-inflammatory cytokines, and continuous cleansing of apoptotic cells. Nevertheless, the exact signaling mechanisms that regulate the phagocytic activity of microglial cells in the SAE are still unclear.

In order to provide new insights for clinical treatment of SAE, in this study, we established the SAE mouse model induced by caecal ligation and puncture (CLP), and then investigated the possible underlying mechanisms of SAE pathogenesis affected by VDAC1.

Materials and methods

Establishment of sepsis-associated encephalopathy (SAE) model and treatment

All animal experiments fully complied with the guidelines of the Institutional Animal Care and Use Committee (IACUC) and were approved by the Ethics Committee for Experimental Animals of our hospital. C57BL/6 mouse (female, 6-8 weeks old, 6 mice per group) were obtain-

ed from Shanghai Model Organisms Company. SAE was induced by caecal ligation and puncture (CLP), and sepsis was established according to the protocol as previously described [30]. The mouse was anesthetized with an intraperitoneal injection of 7% chloral hydrate solution (5 mL/kg). After anesthesia and the preparation of abdominal skin, sterilization was performed by 75% alcohol. Subsequently, the skin of mouse was incised along the medioventral line, and the caecum was ligated 1 cm distance from the apex of cecum to the ileocecal valve. The cecum was then punctured at two sites. Then, a small amount of fecal mass was squeezed out from the punctured sites into the peritoneal cavity. Close abdomen after restoration of the externalized caecum. The mice subjected only to cecectomy without SAE were included in the Sham group. Subsequently, mouse was sacrificed at indicated time points following SAE pathogenesis; the cortex and hippocampal tissues were obtained. Rapamycin (2.5 mg/kg, MedChemExpress, China, HY-10219), Amiloride (7.5 mg/kg, MCE company, HY-B0285), the Ad-Ctrl (Shandong Vigene biosciences company, China), Ad-siVDAC1 (Shandong Vigene biosciences company, China) and Ad-Parkin (Shandong Vigene biosciences company, China) were intracranially injected on the third day after CLP.

Transmission electron microscopic (TEM) analysis

Electron microscopic analysis followed previous published protocols [31]. Briefly, 4% paraformaldehyde and 1% glutaraldehyde were used to fix the isolated brain samples of mouse for 48 h, and these samples were sliced into sections of about 40-60 μm , and mounted onto copper grids. After the fixation, a graded series of concentrations of ethanol (50, 70, 90, 95 and 4 \times 100% each for 15 min) were used to dehydrate, and then these samples were mounted onto copper wire mesh. The ultrathin sections were stained with uranyl acetate and Reynold’s lead citrate, and examined with the Hitachi H500 transmission electron microscope.

Cued and contextual fear conditioning test

The cued and contextual fear conditioning test was applied to evaluate both the hippocampal-dependent and -independent memory. On each

Decreasing the VDAC1 alleviated the cognitive dysfunction

Table 1. Experimental parameters of PCR

Step	Number of cycles	Temp.	Time
Pre-denaturation	1	95°C	3 min
denaturation	40	95°C	15 sec
Annealing and extension		60°C	45 sec

testing day, study subjects occupied the environment of testing room at least 30 min before the test. On the first testing day, each mouse was put into the experimental chamber and went through a pair of the specific-frequency sound (2000 Hz, 85 dB, 30 s) as the tone stimulation (conditioned stimulus, CS) and the foot electric shock (unconditioned stimulus, US). The mouse was moved out from the chamber for 30 s interval after the last stimulation. To strengthen the association, this CS-US training was repeated three times. On the second testing day, contextually conditioned fear test was first conducted. The mouse was put into the same conditioning chamber for 6 min freely without any tones or shock and then moved out from the chamber. They were assessed according to their freezing behaviors. 2 h later, the cued fear conditioning test was conducted. In this test, the mouse was put into another testing chamber with different properties and this chamber did not exist any tone or shock stimulation in the initial 3 min. Later the mouse suffered from the 3 cycles of auditory cue same as those on the first testing day, and freezing time was recorded at each interval. Then the study subjects were moved out from the chamber 60 s after the last tone. The LABmaze controlled fear conditioning system was equipped with a sound-attenuating chamber (1056017, Beijing Zhongshi technology, China), a video camera and the corresponding software to record the freezing time.

Morris water maze

After 7 days of CLP, the Morris water maze (MWM) test was conducted to evaluate the learning and memory abilities of each group of mice. The equipment consisted of a 1.6 m-diameter metal circular pool filled with 60 cm-deep opaque water (reverse osmosis water diluted with black paint) and the pool contained a submerged 10 cm-diameter hidden platform which was fixed 2 cm below the surface of the water. The water temperature was kept

at 23°C. Mice were located on a different quadrant and received training to find the hidden platform for 5 consecutive days. If the platform was not found within 90 s, mouse was guided to stay on the platform for 15 s. The swimming time, speed and latency of mouse were recorded automatically by the overhead camera. After the 5 consecutive days of training, the mouse was allowed to swim freely for 90 s in the pool with the platforms, meanwhile, the times of crossing platform and the time mouse spent in the original quadrant were recorded. All videos and data were recorded and analyzed by using an automatic tracking system.

RNA extraction and quantitative real-time PCR

Hippocampus was detached quickly and immersed in lysis buffer at ratio of 1:6, and then the samples were homogenized by an ultrasound homogenizer. Total RNA extraction was performed according to the supplier's protocol (AM1912, Thermo Scientific). NanoDrop ND-1000 spectrophotometer (Thermo Scientific) was used to evaluate the quantity and purity of RNA. Complementary DNAs were obtained by the reverse transcription reaction with a reverse transcription kit (RR037A, Takara) and applied as templates to determine the expression of target genes by PCR. The reagent was prepared by dispersing 2 µg total RNA into 4 µl 5 × PrimeScript RT Master Mix and diluted up to 20 µL by RNase-free dH₂O. The reverse transcription was performed under 37°C for 30 mins and inactivation of reverse transcriptase under 85°C for 5 seconds. The experimental parameters of PCR are listed in **Table 1**. All the primers (in **Table 2**) were designed by Primer Premier 5.0 software, and synthesized by Sangon Biotech (Shanghai, China).

Immunofluorescent staining

Paraffin-embedded sections of the entire brain were suspended in 20% sucrose solutions until the samples sunk to the bottom of the solution. Tissue mass was embedded with optimal cutting temperature compound and quickly frozen. Then the brain samples were subjected to 30 µm-thin sections, and sections were kept in 4°C PBS solution. The prepared sections were washed three times with PBS, then blocked by the 2% bovine serum albumin for 1 h at the room temperature, and subsequently, the sec-

Decreasing the VDAC1 alleviated the cognitive dysfunction

Table 2. Primer sequences

Gene	Sense primer (5'-3')	Antisense primer (3'-5')
LC3	CGCCGCCTGCAACTCAA	ATCCGTCTTCATCCTTCTCCTGT
P62	CCGCCTGACACCCACTA	CCTTCATCCGAGAAACCC
ATG5	GCCATCAACCGGAAACT	ATGCTCGCTCAGCCACT
ATG7	GGTCGTGTCTGTCAAGTGC	TCCCTGGTGTCCATTAGC
RAC1	CCGTCTTTGACAACTATTCT	ATCCGTCTTCATCCTTCTCCTGT
RhoA	TGACAGCCCTGATAGTTTA	CACAAGATGAGGCACCC
VDAC1	TCTTCAACCAAGGGCTACG	GCCGAGTTGATGTGCT
PINK1	TCTCAAGTCCGACAACATCCT	TTGCCACCACGCTCTACAC
Parkin	CTTCCCAGTGGAGGTCG	GAGGGTTGCTGTTTGC
Gapdh	CAACGGCACAGTCAAGG	CCAGTGGATGCAGGGAT

tions were incubated at 4°C with the primary antibodies. Next day, the sections were washed with PBS three times, 5 min each time. The sections were incubated with the secondary antibodies for 1 h at the room temperature, and washed with PBS three times, followed by staining with DAPI (Beyotime Biotechnology, China) to label cell nuclei. Immunofluorescent images were taken with an inverted fluorescence microscope (Nikon, Japan), and data were analyzed with the Image J software.

Hematoxylin-Eosin (H-E) staining and TUNEL assay

For HE staining, 4% paraformaldehyde solution (Sinopharm, China) was used to fix the brain samples overnight and then the samples were embedded in paraffin. The prepared samples were subjected to 4 µm-thin sections. The brain slices were dewaxed with xylene and with ethanol (Sinopharm, China) for hydration. Then the sections were stained with hematoxylin solution (Sigma-Aldrich) for 5 min and washed with tap water. The slices were lifted and inserted in hydrochloric acid ethanol solution quickly for several times, and then incubated in eosin solution for 2 min. After these procedures, the brain sections were observed and analyzed with the light microscope (Nikon, Japan).

For the TUNEL assay, the paraffin-embedded sections were dewaxed by conventional methods and with gradient concentration of ethanol for hydration, then the slices were washed for 3 times. The brain slices were reacted with protease K working fluid (CloudSec, China) at room temperature for 15 min. Then labeling reactions were performed. The brain sections were observed and analyzed with the light micro-

scope (Nikon, Japan) to evaluate the apoptosis.

Western blotting

Hippocampal mass was lysed with RIPA buffer containing protease inhibitor (4693116001, Roche), and the protein concentration was examined with a BCA protein assay kit (23227, Thermo Scientific). Extracts (30 µg) were separated by SDS-PAGE using 12.5% gels and transferred onto 0.45 µm-thin PVDF membranes (Merck Millipore). Proteins on PVDF membranes were blocked with 5% Bovine serum albumin for 1 h at room temperature, then incubated with primary antibodies (**Table 3**) at 4°C overnight, followed by incubation with secondary antibodies at room temperature for 1 h. Eventually, the protein bands were treated with ECL assay kit (PO018FS; Beyotime Biotechnology), and contrasted by a ChemiDoc XRS imaging system and analyzed by Image Lab software (both Bio-Rad Laboratories, Inc., Hercules, CA, USA).

Antibodies

Antibody information is listed in **Table 3**.

Statistical analysis

All the experiments were carried out for at least three times independently. Data were entered to SPSS (version 24; SPSS (IBM) Inc., Illinois, USA) for analysis. The categorical variants were expressed as number (%). The measurement data were expressed as mean ± standard deviation. A two-way analysis of variance (ANOVA) with post hoc of Tukey's multiple comparison test was used to analyze multiple groups during several days (Morris water maze test). Unpaired Student's t tests or one-way ANOVA was used for two sets of data comparison (SPSS 12.0). Statistical significance was determined at P<0.05.

Results

Cognitive dysfunction, inflammation and microglial cells were increased in CLP-induced SAE mouse model

We established the SAE mouse model induced by CLP to detect whether cognitive impairment

Decreasing the VDAC1 alleviated the cognitive dysfunction

Table 3. Antibody information

Antibodies	Dilution rates	Product codes	Manufacturers
Iba1	1:3000	ab178846	Abcam
GAPDH	1:10000	60004-1-Ig	Wuhan Sanying Biotechnology
LC3	1:2000	14600-1-AP	Wuhan Sanying Biotechnology
P62	1:2000	ab56416	Abcam
ATG5	1:1000	PA5-35201	Invitrogen
ATG7	1:2000	PA5-17216	Invitrogen
β-actin	1:10000	AM4302	Invitrogen
RAC1	1:1000	ab155938	Abcam
RhoA	1:1000	ab187027	Abcam
VDAC1	1:1000	55259-1-AP	Wuhan Sanying Biotechnology
PINK1	1:1000	23274-1-AP	Wuhan Sanying Biotechnology
p-Parkin	1:1000	PA1-4734	Invitrogen
Goat Anti-mouse IgG H&L (HRP)	1:10000	Ab6728	Abcam
Goat Anti-rabbit IgG H&L (HRP)	1:10000	Ab6721	Abcam

was successfully induced secondary to SAE. On the 15th day post-CLP surgery, Morris water maze (MWM) test was conducted in the mice. The results revealed that there was no difference in escape latency between the CLP group and Sham group at the start of the MWM test, while CLP-induced SAE prolonged the latencies on days 2-4 in the MWM test (**Figure 1A**). SAE shortened the time, decreased crossings in the target quadrant and swimming speed (**Figure 1B-D**). These results suggested that cognitive impairment was successfully induced by SAE. In addition, our results showed that the SAE model had a higher malondialdehyde (MDA) level and a stronger 2,7-dichlorodi-hydrofluorescein diacetate (DCFH-DA) fluorescence intensity (**Figure 1E, 1F**). Moreover, HE staining showed that hippocampus DG area of SAE model mice presented obvious neuronal pyknosis, condensed nuclear and disintegrated cell structure. Likewise, more apoptotic cells were found by TUNEL assay (**Figure 1G, 1H**). Western blot and immunofluorescence results showed that the expression of Iba1, a mark gene of microglia cells, was significantly increased in hippocampus of SAE mice (**Figure 1I, 1K, 1L**). These results indicated that the inflammatory response and apoptotic cells significantly increased in SAE pathology.

The mitophagy increased while the efferocytosis decreased in the hippocampus of SAE model

It was reported that mitophagy is related to SAE. Transmission electron microscope (TEM)

results showed that more autophagosome and less efferosomes were found in the SAE model (**Figure 2A, 2D**). The RT-qPCR and the immunoblot results demonstrated that the expressions of LC3, ATG5 and ATG7 were increased, while the p62 was significantly decreased in the hippocampus of SAE model (**Figure 2B, 2C**). Recent studies have manifested that the balance of RhoA/Rac1 has an important effect on efferocytosis [32, 33]. Our study demonstrated that both the expressions of RhoA and Rac1 were decreased in hippocampus of SAE mouse (**Figure 2E, 2F**). These results suggested that mitophagy was increased while efferocytosis was decreased in the pathogenesis of SAE.

Activation of autophagy and inhibition of efferocytosis aggravated the cognitive impairment of mouse

We analyzed the cognitive function of SAE mouse model in the presence of autophagy agonist and efferocytosis inhibitor in order to detect whether autophagy and efferocytosis were related to the cognitive impairment caused by SAE. The results revealed that there was no difference in latency among the groups at the start of the MWM test, and latency decreased significantly on days of 2-4 in six groups. Whether or not under SAE conditions, both activation of autophagy by rapamycin and inhibition of efferocytosis by amiloride prolonged the escape latencies of the mouse (**Figure 3A**).

Similarly, aggravated memory damage of autophagy agonist rapamycin-treated and efferocy-

Decreasing the VDAC1 alleviated the cognitive dysfunction

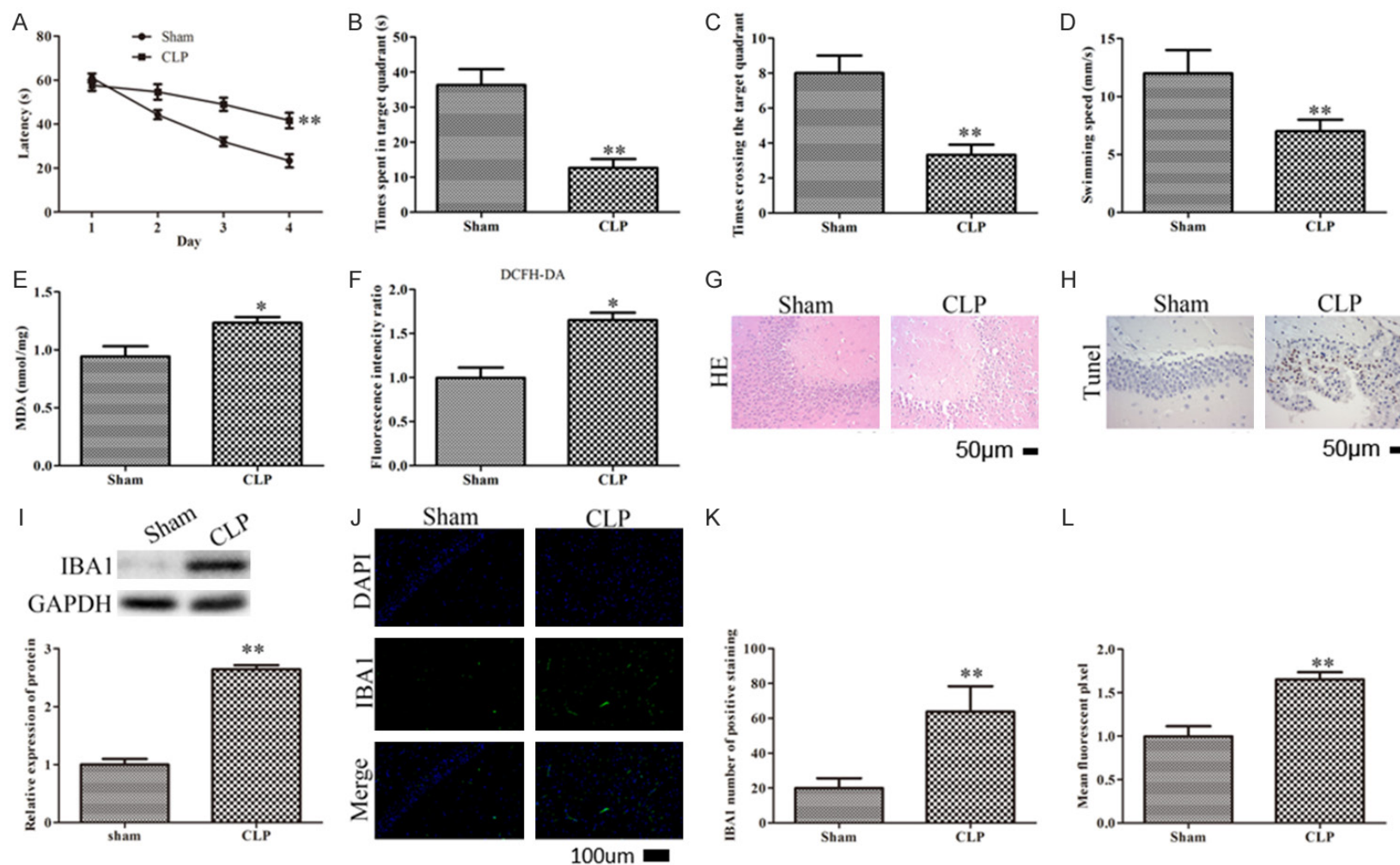


Figure 1. The cognitive function, mitophagy, ROS and inflammatory factor levels in CLP-induced SAE mouse model. For (A-D), Morris water maze test was performed after SAE model was established in C57BL/6 mice for 15 days. (A) In the navigation test, the escape latency was measured to determine the effects of CLP on the spatial learning ability of C57BL/6 mice (n = 10 each group; **P<0.01, compared with the Sham group). (B, C) In the probe test, time spent and times crossing in the target quadrant was measured to determine the effects of CLP on the spatial memory ability of the C57BL/6 mice (n = 10 each group; **P<0.01, compared with the Sham group). (D) Swimming speed was calculated as the ratio of distance traveled/escape latency (n = 10 each group; **P<0.01, compared with the Sham group). (E) The quantification of MDA level (*P<0.05, compared with the Sham group). (F) The normalized fluorescence intensity of DCFH-DA (*P<0.05, compared with the Sham group). (G) Light microscopy of the brain tissues in two groups (haematoxylin and eosin (H, E); 100 ×). (H) The apoptotic cells of hippocampus sections in CLP and Sham group were stained by TUNEL assay kit and observed under light microscopy (100 ×). (I) Western blot analysis and quantitative results indicating the IBA1 protein level in CLP and Sham group (**P<0.01, compared with the Sham group). (J) Iba1 expression levels in brain of CLP group and Sham group (100 ×). (K, L) Quantitative results revealing Iba1 expression levels in brain of CLP group and Sham group (**P<0.01, compared with the Sham group).

Decreasing the VDAC1 alleviated the cognitive dysfunction

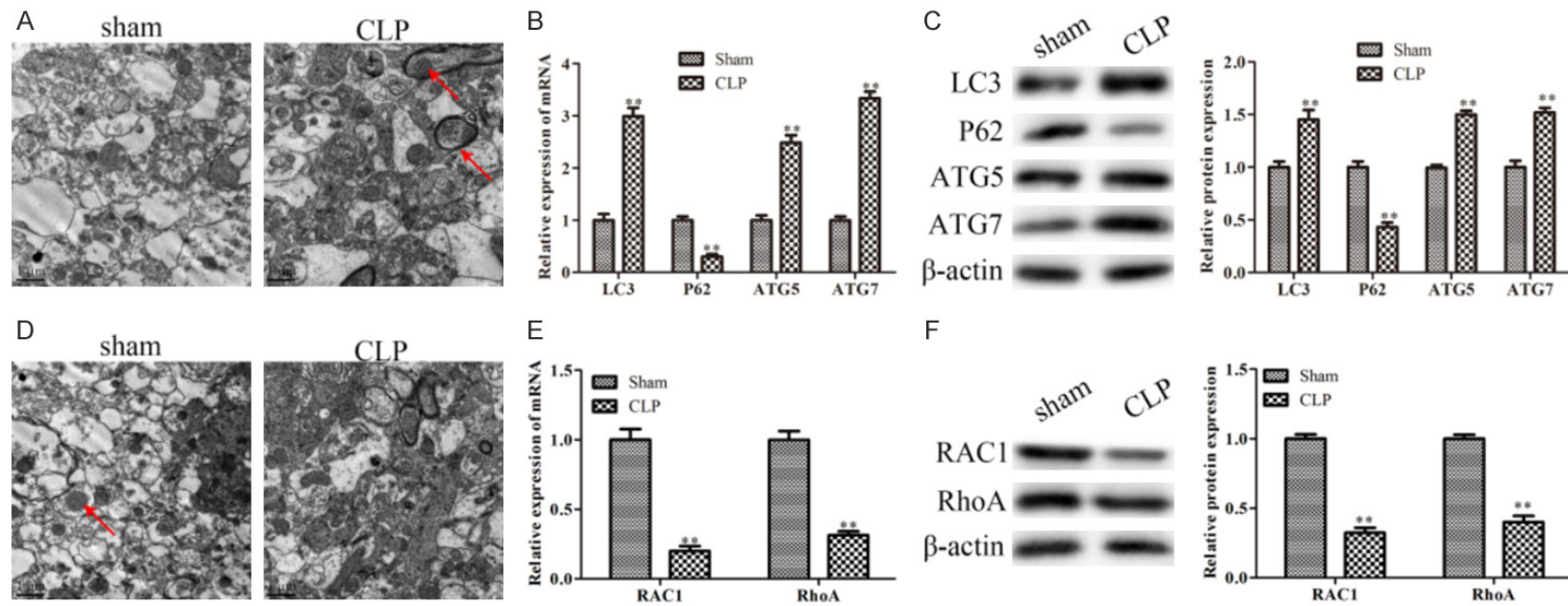


Figure 2. The autophagy and efferocytosis level in CLP-induced SAE mouse model. A. Autophagosomes were observed under the transmission electron microscope, and the red arrows represented the autophagosomes. B. Relative mRNA expression of hall markers of autophagy (** $P < 0.01$, compared with the Sham group). C. Western blot analysis and quantitative results indicating the hall markers of autophagy (** $P < 0.01$, compared with the Sham group). D. Efferosomes were observed under the transmission electron microscope, and the red arrows represented the efferosomes. E. Relative mRNA expression of Rho GTPases (** $P < 0.01$, compared with the Sham group). F. Western blot analysis and quantitative results indicating the Rho GTPases (** $P < 0.01$, compared with the Sham group).

Decreasing the VDAC1 alleviated the cognitive dysfunction

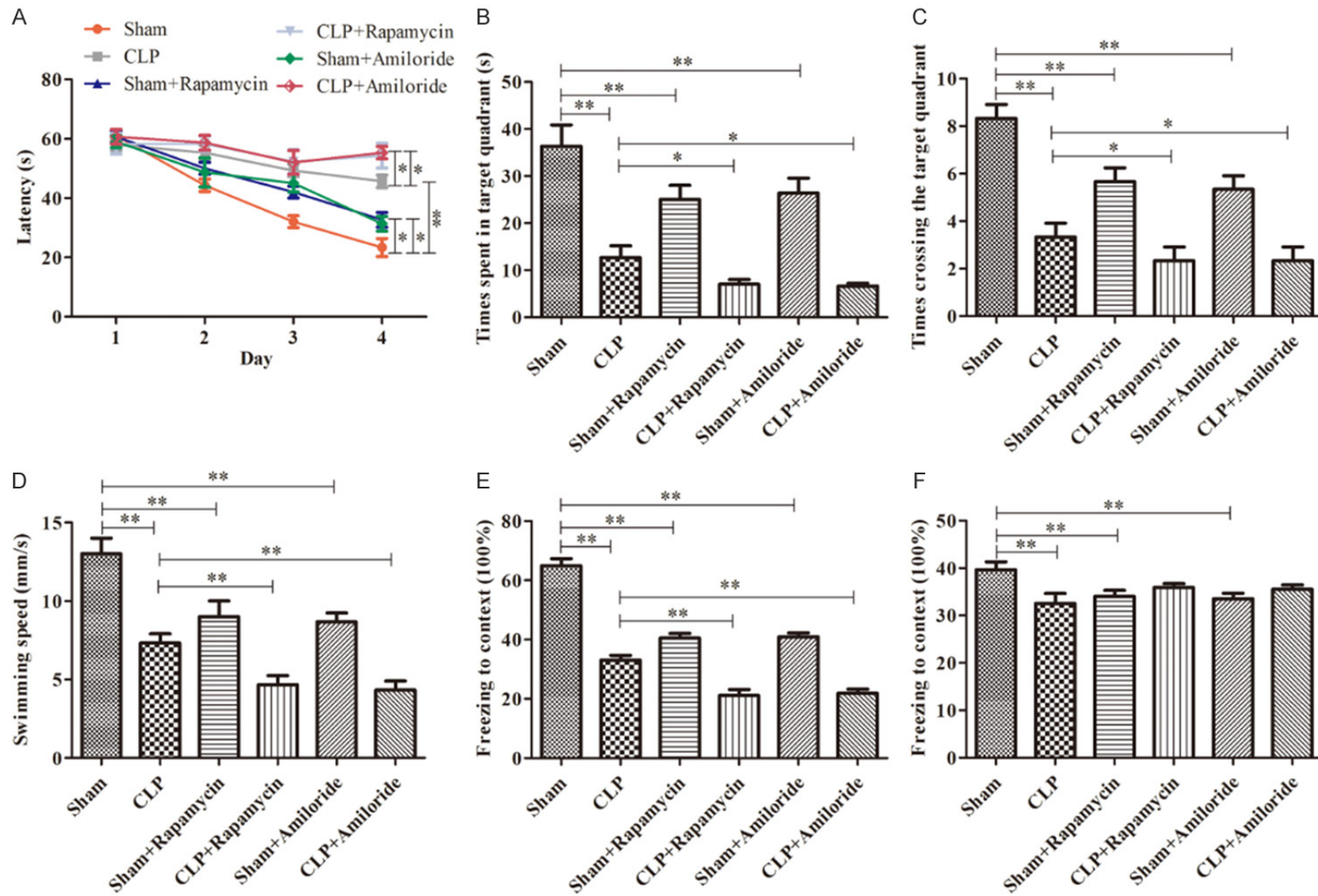


Figure 3. Both autophagy agonist and efferocytosis inhibitor aggravate cognitive dysfunction in CLP-induced SAE mouse model. A. In the navigation test, the escape latency was measured to determine the effects of autophagy agonist (rapamycin) and efferocytosis inhibitor (amiloride) on the spatial learning ability of CLP model mouse (n = 10 each group; *P<0.05, **P<0.01). B, C. In the probe test, time spent and times crossing in the target quadrant were measured to determine the effects of autophagy agonist (rapamycin) and efferocytosis inhibitor (amiloride) on the spatial learning ability of CLP model mouse (n = 10 each group; *P<0.05, **P<0.01). D. Swimming speed was calculated as the ratio of distance traveled/escape latency (n = 10 each group; *P<0.05, **P<0.01). E, F. The effects of autophagy agonist (rapamycin) and efferocytosis inhibitor (amiloride) on the hippocampus-dependent memory and non-hippocampus-dependent memory of CLP model mouse (n = 10 each group; *P<0.05, **P<0.01).

Decreasing the VDAC1 alleviated the cognitive dysfunction

tosis inhibitor amiloride-treated SAE mouse model or Sham mouse was shown by the decreased time and number of crossings in the target quadrant (**Figure 3B, 3C**). Further swimming speed decreased in rapamycin treated and amiloride treated-SAE mouse model (**Figure 3D**). Above results demonstrated that activation of autophagy and inhibition of efferocytosis aggravated the spatial memory damage secondary to SAE or in normal condition.

Moreover, to examine the effect of rapamycin and amiloride on SAE-induced memory impairment, the cued and contextual fear conditioning test was conducted in mice. In both fear conditioning tests, the freezing time of rapamycin-treated and amiloride-treated group significantly decreased (**Figure 3E**), indicating that rapamycin and amiloride aggravated hippocampus-dependent memory and non-hippocampus-dependent memory damage (**Figure 3E, 3F**).

The interaction between autophagy and efferocytosis in the pathogenesis of SAE

Subsequently, we investigated the relationship between autophagy and efferocytosis in the pathogenesis of SAE. The TEM results showed that rapamycin decreased efferosomes in the hippocampus of SAE mouse model (**Figure 4A**). The RT-qPCR and western blot results indicated that rapamycin decreased RhoA and Rac1 expression in both normal and SAE conditions (**Figure 4B, 4C**). Similarly, amiloride increased autophagosomes in the hippocampus of SAE mouse (**Figure 4D**). The RT-qPCR and western blot results indicated that amiloride increased expressions of autophagy mark genes in both normal condition and SAE model (**Figure 4E, 4F**).

Knockdown of VDAC1 alleviated the cognitive dysfunction and memory impairment secondary to SAE in the mouse model

Since the autophagy was involved in the pathogenesis of SAE, in order to find the important regulator in SAE pathology, we checked the VDAC1 expression at the different time points in SAE progression and found that VDAC1 increased significantly after mouse suffered CLP for 7 days (**Figure 5A, 5B**). Immunofluorescence staining of hippocampus of SAE mouse also indicated that VDAC1 increased with IBA1 (**Figure 5C**).

To further explore the effects of VDAC1 on cognitive dysfunction induced by SAE, we injected the VDAC1 siRNA to knock down VDAC1 via peritoneal injection, recorded as the VDAC1⁻ group. The MWM test results revealed that there was no difference in latency among the four groups at the start, and latency decreased significantly over the next three days. Knockdown of VDAC1 prolonged the escape latencies in both normal and CLP-induced SAE conditions (**Figure 5D**).

Knockdown of endogenous VDAC1 in SAE mouse model increased time, crossing numbers and swimming speed in the target quadrant. However no significant difference was found under normal condition after knockdown of VDAC1 (**Figure 5E-G**). Besides, knockdown of VDAC1 in SAE mouse prolonged the freezing time in fear conditioning tests (**Figure 5H, 5I**).

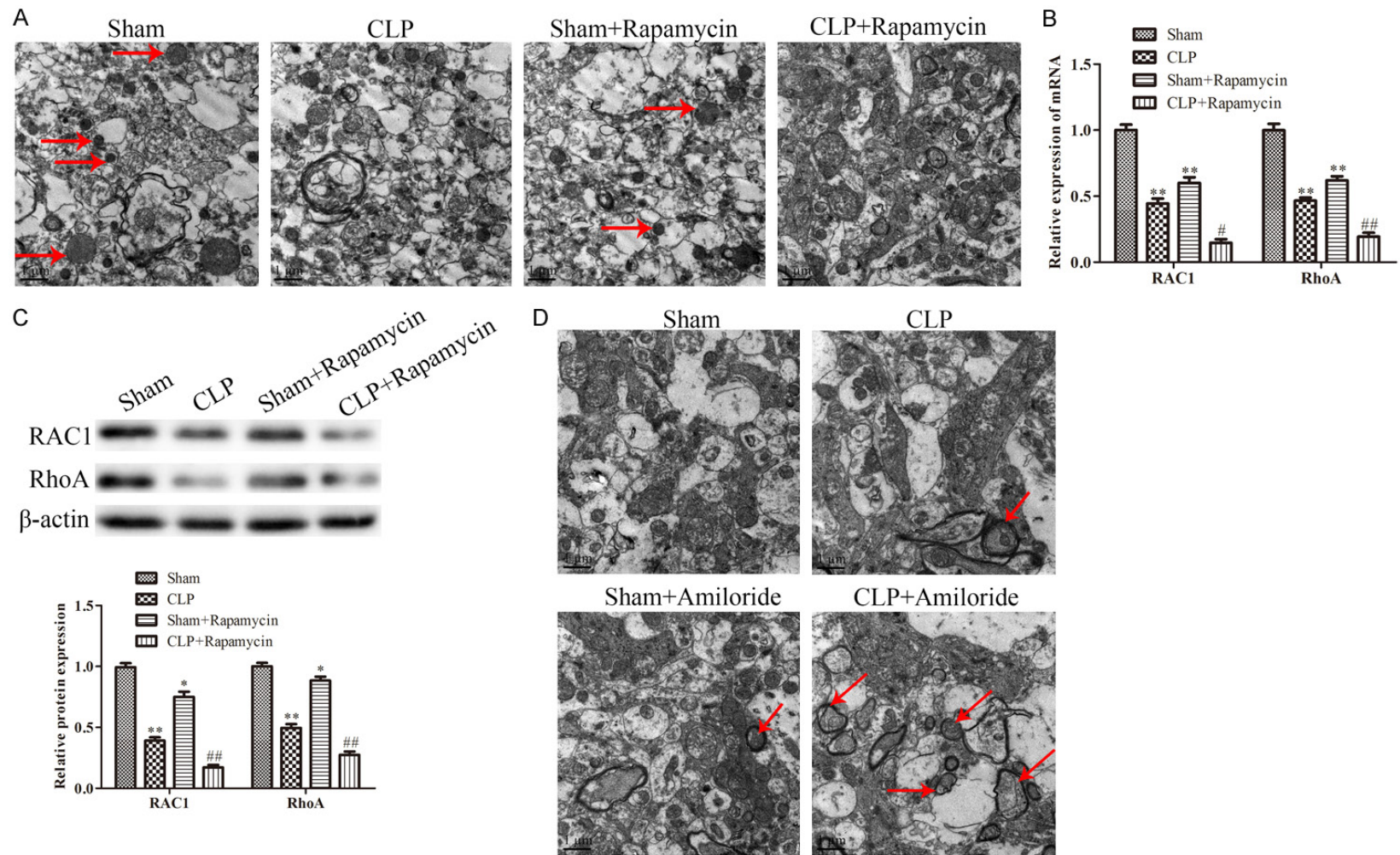
Under TEM observation, we found that knockdown of VDAC1 increased the autophagosomes and decreased efferosomes in the CLP-induced SAE group (**Figure 5J, 5K**), indicating that knock down of VDAC1 improved the cognitive function in the CLP-induced mouse model by inhibiting mitophagy and increasing efferocytosis.

Knockdown of VDAC1 alleviated the cognitive dysfunction and memory impairment in SAE model via PINK1/Parkin mediated mitophagy

PINK1 and Parkin were tightly correlated with mitophagy. Therefore, the role of the PINK1/Parkin signaling pathway in SAE was investigated. We found that CLP group had higher expression of VDAC1 and PINK1 (**Figure 6B**). Further western blotting indicated that knockdown of VDAC1 attenuated the enhancement effect of CLP on PINK1 and p-Parkin (**Figure 6A**).

We injected the Ad-Parkin to the mouse to check the effects of PINK1 and Parkin on cognitive function in SAE mouse. The MWM test data demonstrated that there was no difference in escape latencies among the four groups at the start, and the latencies decreased obviously over the next three days. Further analysis suggested that the presence of Ad-Parkin shortened the prolongation of the latencies induced by knockdown of VDAC1 (**Figure 6C**). In condition of SAE, knockdown of endogenous VDAC1 increased the time, crossing numbers in the target quadrant and swimming speed, while exogenous Parkin partially rever-

Decreasing the VDAC1 alleviated the cognitive dysfunction



Decreasing the VDAC1 alleviated the cognitive dysfunction

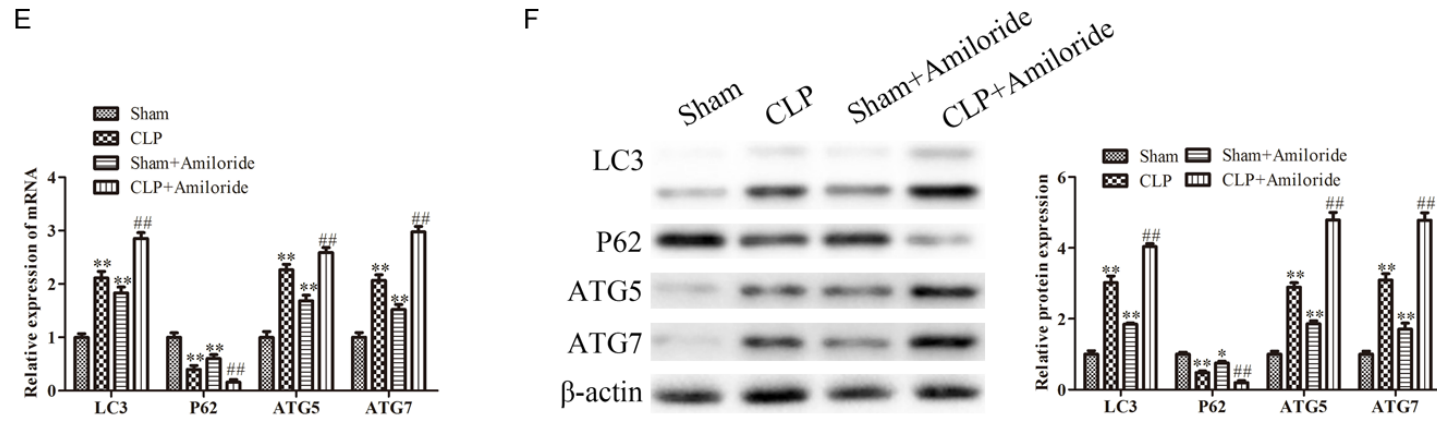
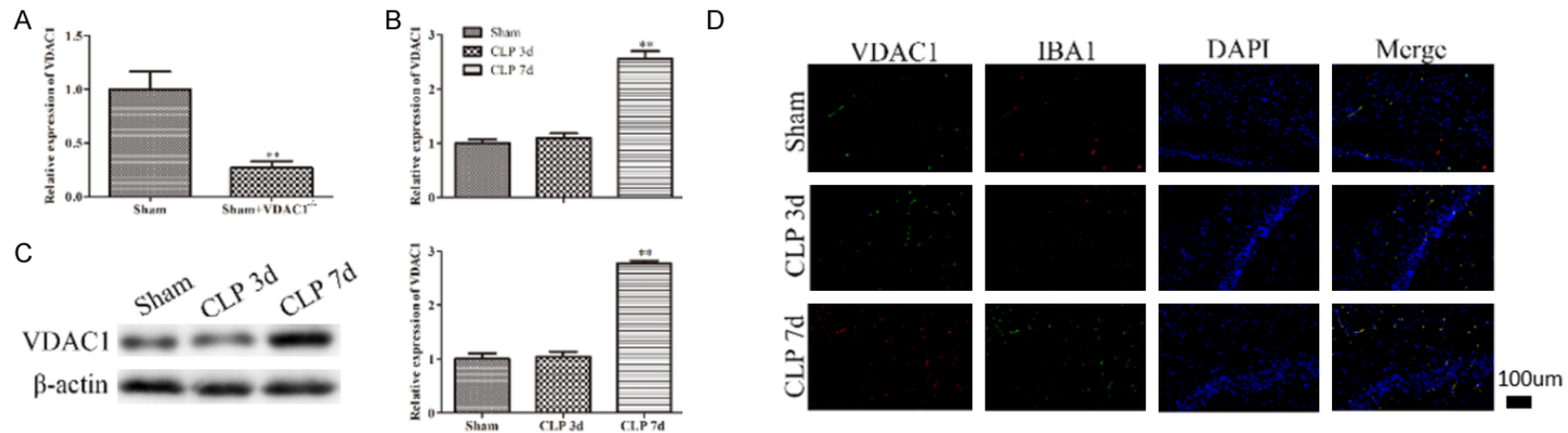


Figure 4. The interaction of autophagy and efferocytosis in CLP-induced SAE mouse model. (A, D) Efferosomes and autophagosomes were observed under the transmission electron microscope. The red arrows represented the efferosomes (A) and autophagosomes (D), respectively. (B) Relative mRNA expression of RhoA and Rac1 indicated the effects of rapamycin on Rho GTPases in the SAE mouse model (** $P < 0.01$ compared with the Sham group, ## $P < 0.01$ compared with the CLP group). (C) Western blot analysis and quantitative results indicated the effects of rapamycin on Rho GTPases in the SAE mouse model (* $P < 0.05$, ** $P < 0.01$ compared with the Sham group; ## $P < 0.01$ compared with the CLP group). (E) Relative mRNA expression of marker genes of autophagy indicated the effects of amiloride on autophagy in the SAE mouse model (** $P < 0.01$ compared with the Sham group; ## $P < 0.01$ compared with the CLP group). (F) Western blot analysis and quantitative results indicated the effects of amiloride on autophagy in the SAE mouse model (* $P < 0.05$, ** $P < 0.01$ compared with the Sham group; ## $P < 0.01$ compared with the CLP group).



Decreasing the VDAC1 alleviated the cognitive dysfunction

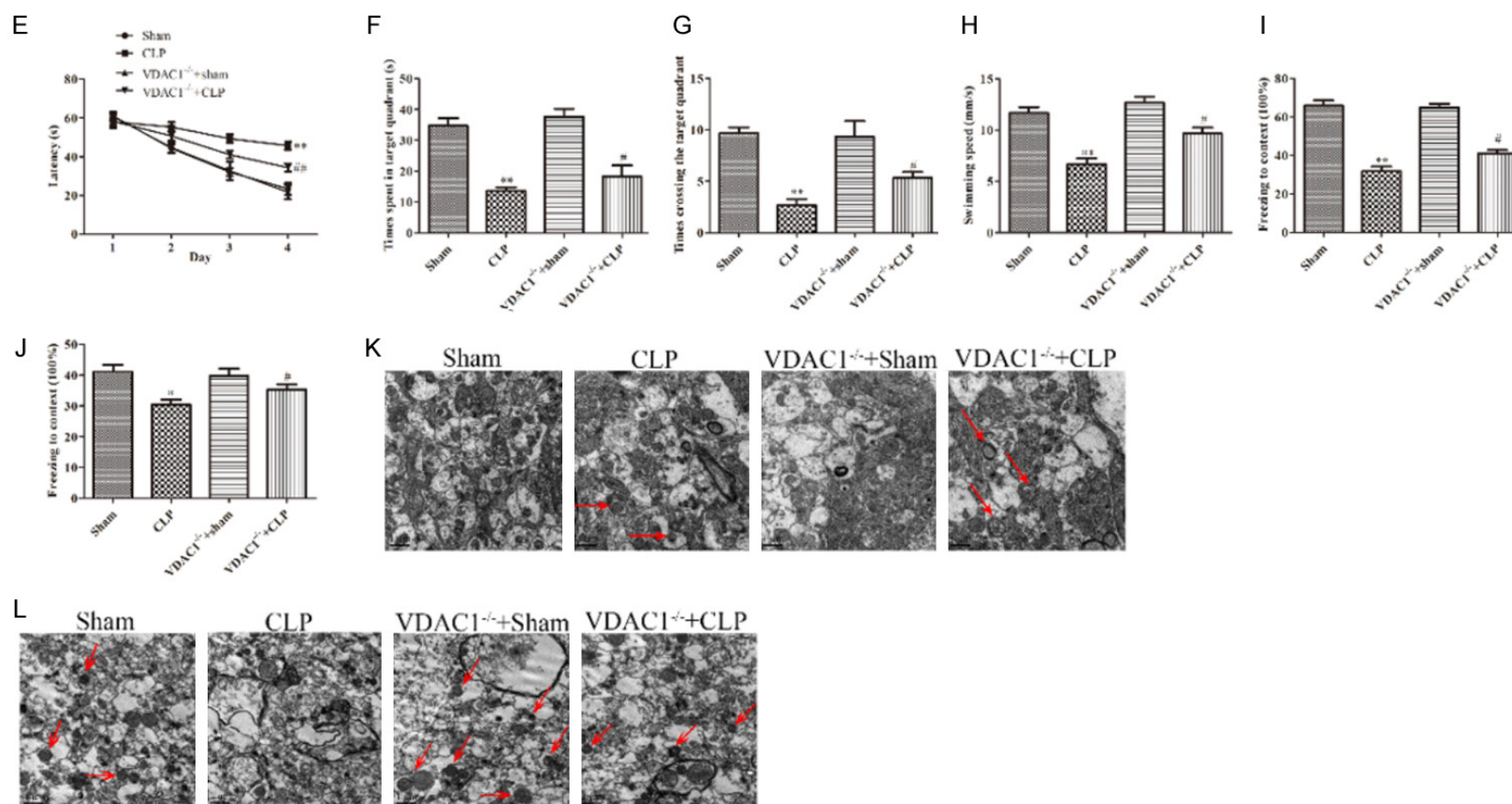


Figure 5. The role of VDAC1 in CLP-induced SAE mouse model. (A, B) Relative mRNA expression and protein level of VDAC1 in CLP-induced SAE mouse model at indicated time point (** $P < 0.01$ compared with the Sham group). (C, D) The co-expression detection of Iba1 and VDAC1 in CLP-induced SAE mouse model at indicated time point in immune fluorescence (** $P < 0.01$ compared with the Sham group, 100 \times). (E) In the navigation test, the escape latency was measured to determine the effects of endogenous VDAC1 on the spatial learning ability of CLP model mouse ($n = 10$ each group; ** $P < 0.01$ compared with Sham group; ## $P < 0.01$ compared with CLP group). (F, G) In the probe test, time spent, times crossing in the target quadrant were measured to determine the effects of endogenous VDAC1 on the spatial learning ability of CLP model mouse ($n = 10$ each group; ** $P < 0.01$ compared with Sham group; # $P < 0.05$ compared with CLP group). (H) Swimming speed was calculated as the ratio of distance traveled/escape latency ($n = 10$ each group; ** $P < 0.01$ compared with Sham group; # $P < 0.05$ compared with CLP group). (I, J) The effects of endogenous VDAC1 on the hippocampus-dependent memory and non-hippocampus-dependent memory of CLP model mouse ($n = 10$ each group; * $P < 0.05$, ** $P < 0.01$ compared with Sham group; # $P < 0.05$, ## $P < 0.01$ compared with CLP group). (K, L) The effects of endogenous VDAC1 on the autophagosomes and efferosomes of CLP model mouse. Autophagosomes and efferosomes were observed under the transmission electron microscopy, the red arrows represented the autophagosomes (K) and efferosomes (L), respectively.

Decreasing the VDAC1 alleviated the cognitive dysfunction

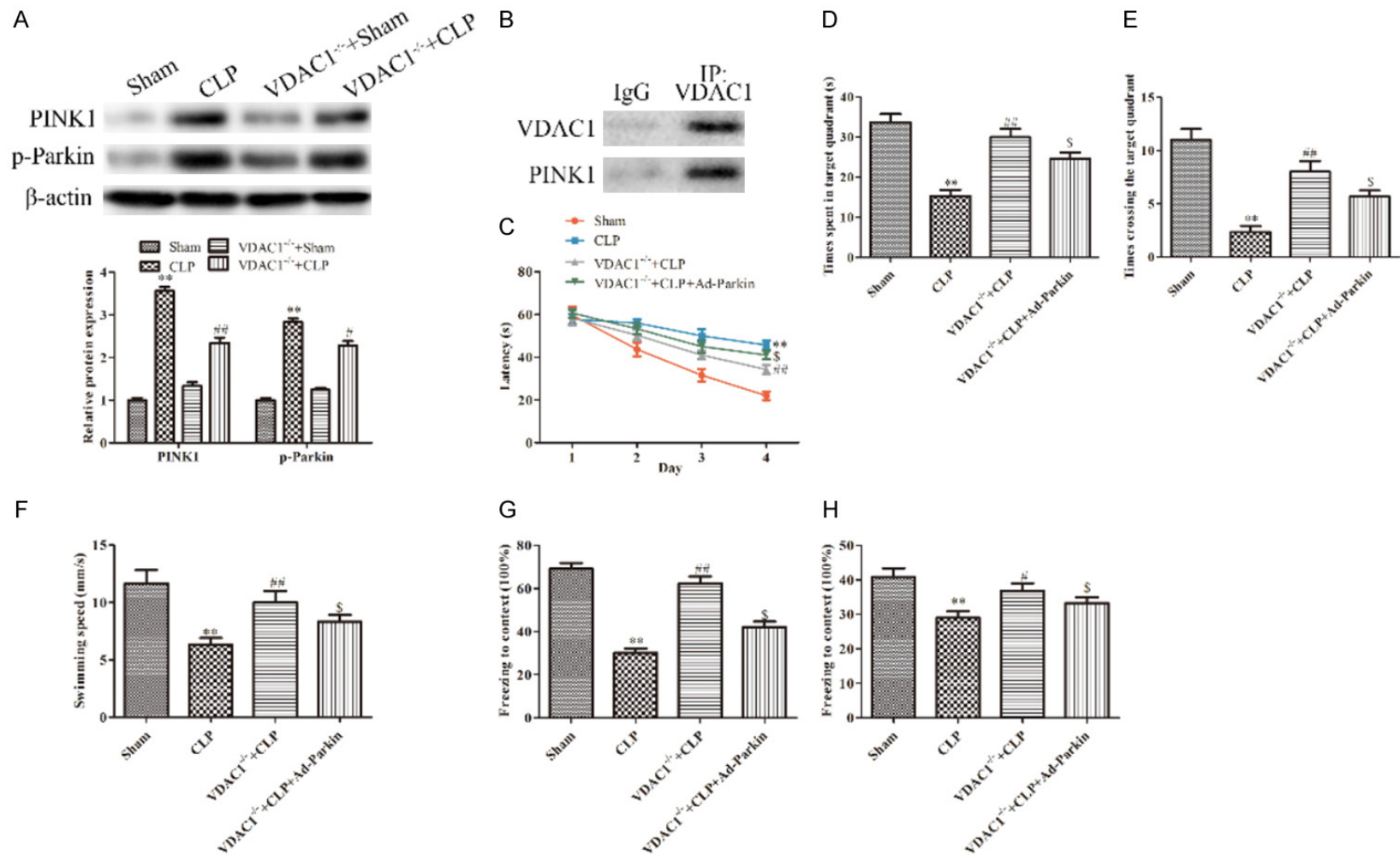


Figure 6. Knockdown of VDAC1 improved the cognitive function in the CLP-induced SAE mouse model in a PINK1/Parkin dependent pathway. **A.** Western blot and quantitative analysis demonstrated that knockdown of VDAC1 attenuated the enhancement effect of CLP on PINK1 and p-Parkin (** $P < 0.01$ compared with Sham group; # $P < 0.05$ compared with CLP group). **B.** VDAC1 and PINK1 protein level in CLP and Sham group. **C.** In the navigation test, the escape latency was measured to determine Parkin and VDAC1 involvement in the spatial learning dysfunction of SAE mouse model ($n = 10$, ** $P < 0.01$ compared with Sham group; ## $P < 0.05$ compared with CLP group; § $P < 0.05$ compared with VDAC1 CLP group). **D, E.** In the probe test, time spent, times crossing in the target quadrant were measured to determine the effects of endogenous VDAC1 on the spatial learning ability of CLP model mouse ($n = 10$ each group; ** $P < 0.01$ compared with Sham group; ## $P < 0.01$ compared with CLP group; § $P < 0.05$ compared with VDAC1 $^{-/-}$ + CLP group). **F.** Swimming speed was calculated as the ratio of distance traveled/escape latency ($n = 10$ each group; ** $P < 0.01$ compared with Sham group; ## $P < 0.01$ compared with CLP group; § $P < 0.05$ compared with VDAC1 $^{-/-}$ + CLP group). **G, H.** The effects of endogenous VDAC1 and Parkin on the hippocampus-dependent memory and non-hippocampus-dependent memory of CLP model mouse ($n = 10$ each group; ** $P < 0.01$ compared with Sham group; # $P < 0.05$ compared with CLP group; § $P < 0.05$ compared with VDAC1 $^{-/-}$ + CLP group).

sed this effect of VDAC1 knockdown (**Figure 6D-F**). Similarly, the freezing time of SAE mouse model with low expression of VDAC1 in both contextual and tone-related cued fear conditioning test was increased, while exogenous Parkin partially reversed the increasing effect of knockdown of VDAC1 (**Figure 6G, 6H**).

The above study results indicated that Parkin partially alleviate the memory impairment effect of knockdown of VDAC1 on SAE, and knockdown of VDAC1 aggravated the cognitive dysfunction and memory impairment in SAE mouse model via a PINK1/Parkin dependent pathway.

Discussion

In this study, a murine SAE model of CLP-induced sepsis was established for exploring the mechanisms of mitophagy and efferocytosis mediated by VDAC1/PINK1/Parkin in pathogenesis of SAE. Mitophagy and efferocytosis were crucial for maintaining intracellular homeostasis [19]. Our results indicated that SAE exacerbated the cognitive impairment in the mouse model. The autophagic response and proinflammatory factors also increased, while the efferocytosis decreased in hippocampus of SAE model. Moreover, we found that the cognitive impairment caused by SAE was aggravated by the rapamycin and amiloride. More importantly, knockdown of VDAC1 alleviated the cognitive dysfunction of SAE model through the PINK1/Parkin pathway. This study illustrated the potential value of the mitophagy and efferocytosis mediated by VADAC1/PINK1/Parkin in the management of cognitive deficits caused by SAE.

The hippocampus is the most vulnerable area to toxins when a diffuse bacterial infection strikes the body. Clinically, advanced SAE patients present acutely mental status changes and are prone to get higher mortality and morbidity than the SAE patients without cognitive disorder [34, 35]. Although several appropriate pathways have been identified to mediate this consequence, such as microscopic brain injury, BBB dysfunction, inflammatory and metabolic changes, the exact regulation of SAE remains to be unclear [36-38]. CLP surgery solution is considered to be a classical animal model for SAE study [39]. In this work, CLP-induced SAE mouse model showed spatial

memory deficits (**Figure 1A-C**), consistent with previous studies. Semmler *et al.* proved that hippocampal atrophy during sepsis produces harmful effects on memory and learning ability [40]. Becher *et al.* reported that inflammatory cytokines outburst aggravates cognitive decline in mouse with SAE [41]. Our investigation obtained the similar results that SAE impaired cognitive function and memory ability.

Mitochondrial function decline is considered as a vital component in secondary multiple organ lesion caused by sepsis [1, 39]. Lambeth *et al.* reported that under the condition of microbial infection in phagocytes and neutrophils, ROS are produced by the NADPH oxidase (NOX) complex in a mitochondria-independent manner [42]. Subsequent findings proved that mitochondria still produces most part of ROS under the condition of infection [43, 44]. Our study proved that more ROS was generated in SAE model (**Figure 1E, 1F**) when mitophagy occurred. In the pathological process of SAE, mitochondrial DNA (mtDNA) released from the injured mitochondria evokes further detriment of oxidative stress and drives innate immune responses [45]. We found that microglial cells were activated in SAE process (**Figure 1I-L**), and the autophagosome increased significantly (**Figure 2A**). Autophagosome was capable of removing the damaged mitochondria in a lysosomal dependent pathway.

During the progression of sepsis, the PINK1 protein accumulates on the OMM and then Parkin is activated by PINK1 and recruited onto mitochondria [46]. The increased activated Parkin protein builds ubiquitin chains on damaged mitochondria to tag them for degradation [47]. The ubiquitin chain binds to the autophagic protein receptor, which binds to LC3 on the autophagosome, to induce mitophagy. Previous research manifested that p62 serves by gathering the injured mitochondria and accelerating mitophagy process [48]. Another study proved that the SQSTM1/p62 protein is one of the key proteins in identification and assemble of damaged mitochondria into autophagosomes [49]. Injured mitochondria are phagocytized by autophagosomes and degraded by lysosomes, which promotes the recovery of septic organ. Our research results demonstrated that autophagy marker genes increased in SAE model (**Figure 2B, 2C**), and rapamycin aggravated the cognitive impair-

ment caused by SAE (**Figure 3**), suggesting that the mitophagy played an important role in SAE pathology. Although VDAC1 regulation of mitochondrial autophagy is controversial [50, 51], a recent study showed that VDAC1 is closely related to mitophagy [52]. In our experiment, VDAC1 functioned as a regulator of mitophagy in a PINK1/Parkin dependent pathway (**Figure 6B**). Several studies reported the role of VDAC1 in sepsis [53]. Our results showed that the VDAC1 expression increased in SAE model (**Figure 5A-C**), and knockdown of VDAC1 improved cognitive function significantly in mouse model (**Figure 5D-H**). Efferocytosis was the core part of regenerative response in brain, which is relevant to maintaining brain tissue homeostasis from neuronal development to neurodegenerative diseases. In this work, we observed that the efferocytosis decreased in CLP-induced SAE model (**Figure 2A**). Recent studies have shown that some autophagy-related genes, such as Beclin1 and LC3, are involved in the regulating phagocytosis [54, 55]. Therefore, we checked the VDAC1 that is closely linked to LC3. It is observed that knockdown of VDAC1 decreased efferocytosis in CLP-induced SAE model (**Figure 5**). Another interesting finding was that the efferocytosis interacted with mitophagy, and the exact mechanism needs further exploring.

The present results suggested that the mitophagy and efferocytosis mediated by VDAC1/PINK1/Parkin might be a promising solution against the pathogenesis of SAE. There are some limitations in this work. The exact mechanism of interaction between efferocytosis and mitophagy is still unclear, which should be further explored in future work. In addition, a number of pre-clinical assessments should also be carried out.

Acknowledgements

This work was supported by the National Natural Science Foundation of China (8197-1872 and 81873954) and Scientific Research Project of Nantong Health Commission (MA2020003). The experimental protocol was established according to the ethical guidelines of the Helsinki Declaration and was approved by the Animal Ethics Committee of Nantong University (S20200314-023).

Disclosure of conflict of interest

None.

Address correspondence to: Hongguang Bao, Department of Anesthesiology, Affiliated Nanjing Hospital of Nanjing Medical University (Nanjing First Hospital), No. 68 Changle Road, Qinhuai District, Nanjing 210006, Jiangsu Province, China. Tel: +86-025-52271041; E-mail: hongguang_bao@163.com; Jie Song, Department of Anesthesiology, The Second Affiliated Hospital of Nantong University, No. 6 North Children Lane, Chongchuan District, Nantong 226001, Jiangsu Province, China. Tel: +86-0513-85061061; E-mail: songjie1004@sina.com

References

- [1] Haileselassie B, Joshi AU, Minhas PS, Mukherjee R, Andreasson KI and Mochly-Rosen D. Mitochondrial dysfunction mediated through dynamin-related protein 1 (Drp1) propagates impairment in blood brain barrier in septic encephalopathy. *J Neuroinflammation* 2020; 17: 36.
- [2] Singer M, Deutschman CS, Seymour CW, Shankar-Hari M, Annane D, Bauer M, Bellomo R, Bernard GR, Chiche JD, Cooper-Smith CM, Hotchkiss RS, Levy MM, Marshall JC, Martin GS, Opal SM, Rubenfeld GD, van der Poll T, Vincent JL and Angus DC. The third international consensus definitions for sepsis and septic shock (Sepsis-3). *JAMA* 2016; 315: 801-810.
- [3] Iwashyna TJ, Ely EW, Smith DM and Langa KM. Long-term cognitive impairment and functional disability among survivors of severe sepsis. *JAMA* 2010; 304: 1787-94.
- [4] Ely EW, Shintani A, Truman B, Speroff T, Gordon SM, Harrell FE Jr, Inouye SK, Bernard GR and Dittus RS. Delirium as a predictor of mortality in mechanically ventilated patients in the intensive care unit. *JAMA* 2004; 291: 1753-1762.
- [5] Rello J, Valenzuela-Sánchez F, Ruiz-Rodríguez M and Moyano S. Sepsis: a review of advances in management. *Adv Ther* 2017; 34: 2393-2411.
- [6] Annane D and Sharshar T. Cognitive decline after sepsis. *Lancet Respir Med* 2015; 3: 61-69.
- [7] Smith M and Meyfroidt G. Critical illness: the brain is always in the line of fire. *Intensive Care Med* 2017; 43: 870-873.
- [8] Iacobone E, Bailly-Salín J, Polito A, Friedman D, Stevens RD and Sharshar T. Sepsis-associated encephalopathy and its differential diagnosis. *Crit Care Med* 2009; 37 Suppl: S331-S336.

Decreasing the VDAC1 alleviated the cognitive dysfunction

- [9] Pickles S, Vigie P and Youle RJ. Mitophagy and quality control mechanisms in mitochondrial maintenance. *Curr Biol* 2018; 28: R170-R185.
- [10] Yamano K, Matsuda N and Tanaka K. The ubiquitin signal and autophagy: an orchestrated dance leading to mitochondrial degradation. *EMBO Rep* 2016; 17: 300-316.
- [11] Pickles S, Vigie P and Youle RJ. Mitophagy and quality control mechanisms in mitochondrial maintenance. *Curr Biol* 2018; 28: R170-R185.
- [12] Youle RJ and Narendra DP. Mechanisms of mitophagy. *Nat Rev Mol Cell Biol* 2011; 12: 9-14.
- [13] Narendra DP, Jin SM, Tanaka A, Suen DF, Gautier CA, Shen J, Cookson MR and Youle RJ. PINK1 is selectively stabilized on impaired mitochondria to activate Parkin. *PLoS Biol* 2010; 8: e1000298.
- [14] Wong YC and Holzbaur EL. Optineurin is an autophagy receptor for damaged mitochondria in parkin-mediated mitophagy that is disrupted by an ALS-linked mutation. *Proc Natl Acad Sci U S A* 2014; 111: E4439-E4448.
- [15] Zhou H, Zhang Y, Hu S, Shi C, Zhu P, Ma Q, Jin Q, Cao F, Tian F and Chen Y. Melatonin protects cardiac microvasculature against ischemia/reperfusion injury via suppression of mitochondrial fission-VDAC1-HK2-mPTP-mitophagy axis. *J Pineal Res* 2017; 63: e12413.
- [16] Geisler S, Holmström KM, Skujat D, Fiesel FC, Rothfuss OC, Kahle PJ and Springer W. PINK1/Parkin-mediated mitophagy is dependent on VDAC1 and p62/SQSTM1. *Nat Cell Biol* 2010; 12: 119-31.
- [17] Zaffagnini G and Martens S. Mechanisms of selective autophagy. *J Mol Biol* 2016; 428: 1714-1724.
- [18] Yu L, Chen Y and Tooze SA. Autophagy pathway: cellular and molecular mechanisms. *Autophagy* 2018; 14: 207-215.
- [19] Galluzzi L, Vitale I, Aaronson SA, Abrams JM, Adam D, Agostinis P, Alnemri ES, Altucci L, Amelio I, Andrews DW, Annicchiarico-Petruzzelli M, Antonov AV, Arama E, Baehrecke EH, Barlev NA, Bazan NG, Bernassola F, Bertrand MJM, Bianchi K, Blagosklonny MV, Blomgren K, Borner C, Boya P, Brenner C, Campanella M, Candi E, Carmona-Gutierrez D, Cecconi F, Chan FK, Chandel NS, Cheng EH, Chipuk JE, Cidlowski JA, Ciechanover A, Cohen GM, Conrad M, Cubillos-Ruiz JR, Czabotar PE, D'Angiolella V, Dawson TM, Dawson VL, De Laurenzi V, De Maria R, Debatin KM, DeBerardinis RJ, Deshmukh M, Di Daniele N, Di Virgilio F, Dixit VM, Dixon SJ, Duckett CS, Dynlacht BD, El-Deiry WS, Elrod JW, Fimia GM, Fulda S, García-Sáez AJ, Garg AD, Garrido C, Gavathiotis E, Golstein P, Gottlieb E, Green DR, Greene LA, Gronemeyer H, Gross A, Hajnoczky G, Hardwick JM, Harris IS, Hengartner MO, Hetz C, Ichijo H, Jäättelä M, Joseph B, Jost PJ, Juin PP, Kaiser WJ, Karin M, Kaufmann T, Kepp O, Kimchi A, Kitsis RN, Klionsky DJ, Knight RA, Kumar S, Lee SW, Lemasters JJ, Levine B, Linkermann A, Lipton SA, Lockshin RA, López-Otín C, Lowe SW, Luedde T, Lugli E, MacFarlane M, Madeo F, Malewicz M, Malorni W, Manic G, Marine JC, Martin SJ, Martinou JC, Medema JP, Mehlen P, Meier P, Melino S, Miao EA, Molkenstein JD, Moll UM, Muñoz-Pinedo C, Nagata S, Nuñez G, Oberst A, Oren M, Overholtzer M, Pagano M, Panaretakis T, Pasparakis M, Penninger JM, Pereira DM, Pervaiz S, Peter ME, Piacentini M, Pinton P, Prehn JHM, Puthalakath H, Rabinovich GA, Rehm M, Rizzuto R, Rodrigues CMP, Rubinsztein DC, Rudel T, Ryan KM, Sayan E, Scorrano L, Shao F, Shi Y, Silke J, Simon HU, Sistigu A, Stockwell BR, Strasser A, Szabadkai G, Tait SWG, Tang D, Tavernarakis N, Thorburn A, Tsujimoto Y, Turk B, Vanden Berghe T, Vandenabeele P, Vander Heiden MG, Villunger A, Virgin HW, Vousden KH, Vucic D, Wagner EF, Walczak H, Wallach D, Wang Y, Wells JA, Wood W, Yuan Y, Zakeri Z, Zhitovskiy B, Zitvogel L, Melino G and Kroemer G. Molecular mechanisms of cell death: recommendations of the Nomenclature Committee on Cell Death 2018. *Cell Death Differ* 2018; 25: 486-541.
- [20] Cummings RJ, Barbet G, Bongers G, Hartmann BM, Gettler K, Muniz L, Furtado GC, Cho J, Lira SA and Blander JM. Different tissue phagocytes sample apoptotic cells to direct distinct homeostasis programs. *Nature* 2016; 539: 565-569.
- [21] Chung WS, Clarke LE, Wang GX, Stafford BK, Sher A, Chakraborty C, Joung J, Foo LC, Thompson A, Chen C, Smith SJ and Barres BA. Astrocytes mediate synapse elimination through MEGF10 and MERTK pathways. *Nature* 2013; 504: 394-400.
- [22] Medina CB and Ravichandran KS. Do not let death do us part: 'find-me' signals in communication between dying cells and the phagocytes. *Cell Death Differ* 2016; 23: 979-989.
- [23] Elliott MR, Chekeni FB, Trampont PC, Lazarowski ER, Kadl A, Walk SF, Park D, Woodson RI, Oostankovich M, Sharma P, Lysiak JJ, Harden TK, Leitinger N and Ravichandran KS. Nucleotides released by apoptotic cells act as a find-me signal to promote phagocytic clearance. *Nature* 2009; 461: 282-286.
- [24] Segawa K, Kurata S, Yanagihashi Y, Brummelkamp TR, Matsuda F and Nagata S. Caspase-mediated cleavage of phospholipid flippase for apoptotic phosphatidylserine exposure. *Science* 2014; 344: 1164-1168.
- [25] Suzuki J, Denning DP, Imanishi E, Horvitz HR and Nagata S. Xk-related protein 8 and CED-8

Decreasing the VDAC1 alleviated the cognitive dysfunction

- promote phosphatidylserine exposure in apoptotic cells. *Science* 2013; 341: 403-406.
- [26] Chao MP, Weissman IL and Majeti R. The CD47-SIRP α pathway in cancer immune evasion and potential therapeutic implications. *Curr Opin Immunol* 2012; 24: 225-232.
- [27] Veillette A and Chen J. SIRP α -CD47 immune checkpoint blockade in anticancer therapy. *Trends Immunol* 2018; 39: 173-184.
- [28] Larson SR, Atif SM, Gibbings SL, Thomas SM, Prabagar MG, Danhorn T, Leach SM, Henson PM and Jakubzick CV. Ly6C(+) monocyte efferocytosis and cross-presentation of cell-associated antigens. *Cell Death Differ* 2016; 23: 997-1003.
- [29] Hamers AAJ, Dinh HQ, Thomas GD, Marcovecchio P, Blatchley A, Nakao CS, Kim C, McSkimming C, Taylor AM, Nguyen AT, McNamara CA and Hedrick CC. Human monocyte heterogeneity as revealed by high-dimensional mass cytometry. *Arterioscler Thromb Vasc Biol* 2019; 39: 25-36.
- [30] Rittirsch D, Huber-Lang MS and Flierl MA. Immunodesign of experimental sepsis by cecal ligation and puncture. *Nat Protoc* 2009; 4: 31-36.
- [31] Chiang T, Chen C and Tseng P. Bismuth salts with versus without acid suppression for *Helicobacter pylori* infection: a transmission electron microscope study. *Helicobacter* 2021; 26: e12801.
- [32] Akhtar N, Li W, Mironov A and Streuli CH. Rac1 controls both the secretory function of the mammary gland and its remodeling for successive gestations. *Dev Cell* 2016; 38: 522-535.
- [33] Richens TR, Linderman DJ, Horstmann SA, Lambert C, Xiao YQ, Keith RL, Boé DM, Morimoto K, Bowler RP, Day BJ, Janssen WJ, Henson PM and Vandivier RW. Cigarette smoke impairs clearance of apoptotic cells through oxidant-dependent activation of RhoA. *Am J Respir Crit Care Med* 2009; 179: 1011-1021.
- [34] Iwashyna TJ, Ely EW, Smith DM and Langa KM. Long-term cognitive impairment and functional disability among survivors of severe sepsis. *JAMA* 2010; 304: 1787-1794.
- [35] Jackson JC, Hart RP, Gordon SM, Shintani A, Truman B, May L and Ely EW. Six-month neuropsychological outcome of medical intensive care unit patients. *Crit Care Med* 2003; 31: 1226-1234.
- [36] Adam N, Kandelman S, Mantz J, Chrétien F and Sharshar T. Sepsis-induced brain dysfunction. *Expert Rev Anti Infect Ther* 2013; 11: 211-221.
- [37] Flierl MA, Stahel PF, Rittirsch D, Huber-Lang M, Niederbichler AD, Hoesel LM, Touban BM, Morgan SJ, Smith WR, Ward PA and Ipaktchi K. Inhibition of complement C5a prevents breakdown of the blood-brain barrier and pituitary dysfunction in experimental sepsis. *Crit Care* 2009; 13: R12.
- [38] Wolf SA, Boddeke HW and Kettenmann H. Microglia in physiology and disease. *Annu Rev Physiol* 2017; 79: 619-643.
- [39] Martínez-García JJ, Martínez-Banaclocha H, Angosto-Bazarra D, de Torre-Minguela C, Baroja-Mazo A, Alarcón-Vila C, Martínez-Alarcón L, Amores-Iniesta J, Martín-Sánchez F, Ercole GA, Martínez CM, González-Lisorge A, Fernández-Pacheco J, Martínez-Gil P, Adriouch S, Koch-Nolte F, Luján J, Acosta-Villegas F, Parrilla P, García-Palenciano C and Pelegrin P. P2X7 receptor induces mitochondrial failure in monocytes and compromises NLRP3 inflammasome activation during sepsis. *Nat Commun* 2019; 10: 2711.
- [40] Semmler A, Widmann CN, Okulla T, Urbach H, Kaiser M, Widman G, Mormann F, Weide J, Fliessbach K, Hoefl A, Jessen F, Putensen C and Heneka MT. Persistent cognitive impairment, hippocampal atrophy and EEG changes in sepsis survivors. *J Neurol Neurosurg Psychiatry* 2013; 84: 62-69.
- [41] Becher B, Spath S and Goverman J. Cytokine networks in neuroinflammation. *Nat Rev Immunol* 2017; 17: 49-59.
- [42] Lambeth JD and Neish AS. Nox enzymes and new thinking on reactive oxygen: a double-edged sword revisited. *Annu Rev Pathol* 2014; 9: 119-145.
- [43] Saleh J, Peyssonnaux C, Singh KK and Edeas M. Mitochondria and microbiota dysfunction in COVID-19 pathogenesis. *Mitochondrion* 2020; 54: 1-7.
- [44] Khan S, Raj D, Jaiswal K and Lahiri A. Modulation of host mitochondrial dynamics during bacterial infection. *Mitochondrion* 2020; 53: 140-149.
- [45] Keshavarz-Bahaghighat H, Darwesh AM, Sosnowski DK and Seubert JM. Mitochondrial dysfunction and inflammaging in heart failure: novel roles of CYP-derived epoxy lipids. *Cells* 2020; 9: 1565.
- [46] Okatsu K, Oka T, Iguchi M, Imamura K, Kosako H, Tani N, Kimura M, Go E, Koyano F, Funayama M, Shiba-Fukushima K, Sato S, Shimizu H, Fukunaga Y, Taniguchi H, Komatsu M, Hattori N, Mihara K, Tanaka K and Matsuda N. PINK1 autophosphorylation upon membrane potential dissipation is essential for Parkin recruitment to damaged mitochondria. *Nat Commun* 2012; 3: 1016.
- [47] Koyano F, Okatsu K, Kosako H, Tamura Y, Go E, Kimura M, Kimura Y, Tsuchiya H, Yoshihara H, Hirokawa T, Endo T, Fon EA, Trempe JF, Saeki Y, Tanaka K and Matsuda N. Ubiquitin is phos-

Decreasing the VDAC1 alleviated the cognitive dysfunction

- phorylated by PINK1 to activate parkin. *Nature* 2014; 510: 162-166.
- [48] Okatsu K, Saisho K, Shimanuki M, Nakada K, Shitara H, Sou YS, Kimura M, Sato S, Hattori N, Komatsu M, Tanaka K and Matsuda N. p62/SQSTM1 cooperates with Parkin for perinuclear clustering of depolarized mitochondria. *Genes Cells* 2010; 15: 887-900.
- [49] Ashrafi G and Schwarz TL. The pathways of mitophagy for quality control and clearance of mitochondria. *Cell Death Differ* 2013; 20: 31-42.
- [50] Narendra D, Kane LA, Hauser DN, Fearnley IM and Youle RJ. p62/SQSTM1 is required for Parkin-induced mitochondrial clustering but not mitophagy; VDAC1 is dispensable for both. *Autophagy* 2010; 6: 1090-1106.
- [51] Geisler S, Holmström KM, Skujat D, Fiesel FC, Rothfuss OC, Kahle PJ and Springer W. PINK1/Parkin-mediated mitophagy is dependent on VDAC1 and p62/SQSTM1. *Nat Cell Biol* 2010; 12: 119-131.
- [52] Chopra M, Golden HB, Mullapudi S, Dowhan W, Dostal DE and Sharma AC. Modulation of myocardial mitochondrial mechanisms during severe polymicrobial sepsis in the rat. *PLoS One* 2011; 6: e21285.
- [53] Chiang N, Shinohara M, Dalli J, Mirakaj V, Kibi M, Choi AM and Serhan CN. Inhaled carbon monoxide accelerates resolution of inflammation via unique proresolving mediator-heme oxygenase-1 circuits. *J Immunol* 2013; 190: 6378-6388.
- [54] Berger SB, Romero X, Ma C, Wang G, Faubion WA, Liao G, Compeer E, Keszei M, Rameh L, Wang N, Boes M, Regueiro JR, Reinecker HC and Terhorst C. SLAM is a microbial sensor that regulates bacterial phagosome functions in macrophages. *Nat Immunol* 2010; 11: 920-927.
- [55] Berger SB, Romero X and Ma C. SLAM is a microbial sensor that regulates bacterial phagosome functions in macrophages. *Nat Immunol* 2010; 11: 920-927.